KeAi

CHINESE ROOTS
GLOBAL IMPACT

Contents lists available at ScienceDirect

Petroleum Science

journal homepage: www.keaipublishing.com/en/journals/petroleum-science



Original Paper

Flow characteristics of shale oil and their geological controls: A case study of the Lucaogou Formation in the Jimsar Sag, Junggar Basin



Jia-Qi Liu^{a,b}, Jun-Qian Li^{a,b,*}, Zhao-Jing Song^{a,b}, An-Chao Shen^{a,b}

- ^a National Key Laboratory of Deep Oil and Gas, China University of Petroleum (East China), Qingdao, 266580, Shandong, China
- b School of Geosciences, China University of Petroleum (East China), Qingdao, 266580, Shandong, China

ARTICLE INFO

Article history: Received 31 July 2024 Received in revised form 28 March 2025 Accepted 19 June 2025 Available online 24 June 2025

Edited by Xi Zhang and Jie Hao

Keywords: Shale oil Flow simulation experiment Flow characteristic Pore throat structure Lucaogou Formation

ABSTRACT

The Lucaogou Formation in Jimsar has a significant development potential due to its massive shale oil resources. Nevertheless, the complex and heterogeneous lithology, coupled with unclear flow mechanisms, poses a challenge in effectively predicting its development potential. Therefore, it is crucial to clarify the flow characteristics of shale oil and its controlling factors. In this study, we used a flow simulation experiment to investigate the flow characteristics of different samples under various temperatures and confining stresses and quantitatively evaluated flow characteristics using threshold pressure gradient and total loss of flow rate. Additionally, by combining scanning electron microscopy and mercury intrusion capillary pressure techniques for pore structure characterization, and the relationship between microscopic pore structure and flow parameters was discussed. The findings indicate that rock composition and pore throat structure collaboratively control shale oil flow. Mesopores and macropores primarily develop between dolomite or albite, leading to well-developed pore throat structure with larger average throat radius, lower displacement pressure, and better reservoir quality, enhancing shale oil flowability. Dolomitic siltstone often exhibits these characteristics, making it a favorable lithology for shale oil flow. This study reveals the flow mechanism of shale oil under the action of reservoir physical properties, material compositions, temperatures and confining stresses, summarizes the geological characteristics of advantageous reservoirs. It provides theoretical support for layer selection and efficient development of shale oil reservoirs in the Lucaogou Formation of the Jimsar. © 2025 The Authors. Publishing services by Elsevier B.V. on behalf of KeAi Communications Co. Ltd. This is an open access article under the CC BY license (http://creativecommons.org/licenses/by/4.0/).

1. Introduction

The exploration and exploitation of unconventional resources has steadily become a hot topic in many nations due to the rapidly rising global energy demand, the ongoing use of conventional oil and gas resources, and the shale oil and gas revolution in the United States (Zou et al., 2020a; Jin et al., 2023; Li et al., 2024a). China is rich in continental shale oil resources, and preliminary estimates show that the total reserves are about 28.3 billion tons (Bai et al., 2022; Zhao et al., 2023). It has become an important strategic target in unconventional oil and gas exploration and development in recent years, which is of great significance to safeguarding national energy security (Hou et al., 2017; Yang et al.,

E-mail address: lijunqian@upc.edu.cn (J.-Q. Li).

Peer review under the responsibility of China University of Petroleum (Beijing).

2019; Zou et al., 2020b; Sun et al., 2023). However, the ultra-low permeability and the significant contact force between the fluid inside the reservoir and the pore wall in the shale formation have made it difficult to develop shale oil (Liu et al., 2022; Li et al., 2022; Li and Cai, 2023; Wang et al., 2023).

The place where shale oil flow occurs is the pore network space under the control of pore throat, the flow law of shale oil is affected by microscopic pore structure, macroscopic physical properties, rock composition and effective stress (Li et al., 2020; Du et al., 2023; Lin et al., 2023). Furthermore, shale pores have a huge specific surface area and the fluid molecules near the wall area will form a viscous layer with strong adsorption force between the fluid and the surface, which increases the friction coefficient of liquid flow and hinders the flow of fluid, resulting in threshold pressure gradient (TPG) and nonlinear flow characteristics (Wang and Sheng, 2017; Dang et al., 2022; Jia et al., 2024).

Non-linear flow characteristics are important manifestations of micro-nano pore structure in tight reservoirs. Li et al. (2017) introduced total loss of flow rate (ΔS) and permeability change rate

^{*} Corresponding author.

to quantitatively evaluate the dynamic process of gas flow when studying the flow process of adsorbed gas in different rank coals. On this basis, Lin et al. (2022) characterized the degree of deviation from Darcy flow in shale samples from the Jiyang Depression using parameter ΔS . The closer the ΔS value approaches 0, the more apparent the linear characteristics become. The TPG is an important parameter to describe the flow capacity of the reservoir. which is common in the fluid flow process of tight reservoirs. Barenblatt et al. (1960) found that fluid can flow only when the driving force of fluid flow in rock is greater than a certain value, and proposed the concept of TPG for the first time. The presence of TPG, which happens often in shale oil reservoirs, drastically reduces well productivity and thus it is important to clarify the TPG. The TPG in the reservoirs of non-linear fluid flow has been extensively studied. Zhang et al. (2022b) modified the gravity term in the Darcy flow equation, applied the non-Darcy flow effect to the simulation process, and proposed a model for obtaining the TPG. Yue et al. (2024) obtained the TPG through the permeability obtained from core displacement experiments. In addition, the value of TPG can also be obtained by the intercept of the flow curve. In the same way, Teng et al. (2023) also used this way for the study of nonlinear Darcy flow.

The Lucaogou Formation is developed in the delta front and lake sedimentary environment, the characteristics of fine grain size, complex lithology, large number of thin interbedded layers, frequent source-reservoir interbedded layers, strong heterogeneity and poor reservoir porosity and permeability lead to lower production than planned expectations (Zhang et al., 2019; Wang et al., 2019; Yu et al., 2023). Accurate prediction of shale oil production requires an in-depth understanding of the shale oil flow mechanism, however, the flow process of shale oil manifests a prominent multi-scale effect, and the flow mechanism is still unclear, posing significant challenges in elucidating the intricate interplay between flow characteristics and reservoir properties. To address this issue, this study thoroughly examines the physical properties, pore throat structure, and other features of nine samples from the Lucaogou Formation in Jimsar, utilizing mercury intrusion capillary pressure (MICP) and scanning electron microscopy (SEM) techniques. Additionally, a physical simulation experiment is conducted to assess flow behavior. Based on the flow characteristics observed in samples of diverse types and lithologies, a quantitative evaluation is performed using TPG and ΔS . Finally, a comprehensive analysis is conducted on the intricate relationship between reservoir characteristics and flow properties, culminating in the identification and summary of favorable flow reservoirs within the Lucaogou Formation in Jimsar.

2. Experiment and methodology

2.1. Samples and experiments

2.1.1. Samples

The Jimsar Sag, a secondary tectonic unit in the eastern uplift of the Junggar Basin, spans from the Shaqi Uplift in the north to the Fukang Fault zone in the south, bordered by the Santai and Guxi uplifts to the west and east, covering approximately 1278 km². It is a dustpan-like sag developed on the folded basement of the Middle Carboniferous. The terrain gradually slopes from west to east, with the stratum thinning eastward (Wang et al., 2022). The Lucaogou Formation in Jimsar, deposited in an offshore saline lake environment, underwent processes like dolomitization, volcanic activity, and terrigenous clastic deposition, yielding a mixed shale featuring complex lithology, mineral composition, and strong heterogeneity. Due to southern provenance, the southern section of the Lucaogou Formation has a higher sandy content, while mud

content rises northward, along with thicker mudstone layers (Ding et al., 2023). Based on lithological variations, the Lucaogou Formation is divided into the lower member (P_2l_1) and the upper member (P_2l_2). The upper sweet spot comprises siltstone, argillaceous siltstone, and dolomite, while the lower sweet spot is primarily dolomitic siltstone (Zhao et al., 2020; Yang et al., 2023).

Nine samples were selected from five wells of the Lucaogou Formation in the Jimsar Sag (Fig. 1(c)). The sampling depth ranged from 2674.44 to 3693.41 m, featuring lithologies including dolomitic siltstone, doloarenite, siltstone, dolomicrite and mudstone. The composition consisted mainly of terrigenous detritus, carbonate minerals and organic matter (OM). The samples had a diameter of approximately 24.5 mm and lengths ranging from 27.67 to 55.80 mm. Most samples had good porosity (1.8%–15.48%, 11.76% on average), but the permeability were extremely low (0.0046–0.095 mD, 0.0375 mD on average), belonging to the medium porosity and ultra-low permeability reservoir. Details of the sample information are presented in Table 1.

2.1.2. Experiments

The X-Ray Diffractometer (XRD) test was carried out according to the standard SY/T 5163-2018. The processed powder samples were placed in the Rigaku Ultima IV X-ray diffractometer for testing. The mineral types were judged by the crystal structure, and the mineral phase contents were judged by the strength of the diffraction peak. The pore throat structure of test samples were processed into core plugs with a diameter of 24.5 mm and a height of 2 cm, followed by solvent extraction and drying. The treated samples were placed in the AutoPore IV 9510 mercury porosimeter, and the liquid mercury was injected into the sample under high pressure for detection. The detection steps were in accordance with the Chinese Oil and Gas Industry Standard, SY/T 5346-2005. The FEI Helios Nanolab 600i was used to analyze the pore characteristics of samples. Before the test, samples were processed into a cube of about 1 cm³, and the surface of them were polished with sandpaper to obtain a smooth surface, and then samples were fixed on the stage for milling. A carbon layer was coated on the surface of the samples after milling to improve the conductivity of the samples and obtain high-quality image information. In order to understand the mineral information, Energy Dispersive Spectrometer (EDS) analysis was also carried out.

The differential pressure-steady state flow method was used to test the flow experiment at different temperatures (40 °C, 50 °C) and different confining stress conditions (10, 15, 20, 25, 30 MPa) using the MR-DD high temperature and pressure displacement device (National Key Laboratory of Deep Oil and Gas). The inlet pressure was provided by the double cylinder constant pressure constant flow pump. The flow rate in the constant speed mode ranged from 0.01 to 17 mL/min, with an accuracy of $< \pm$ 0.3%. The constant pressure mode operated within a pressure range of 0-40 MPa, with an accuracy of 0.01 MPa. The inlet pump was connected to the pressure converter to convert the pressure from the pressure liquid to the flow fluid. The pressure parameter was adjusted by the pressure reducing valve, and the pressure was supplied by the air pump. The confining stress pump exhibited a setting range of 0-40 MPa, with an accuracy of 0.1 MPa, ensuring precise control of experimental conditions. The pressure converter featured a temperature setting range of 10-80 °C, maintaining a control accuracy of 0.1 °C. The computer input and controlled the confining stress and the sample temperature in the rock core holder. The high-precision volumometer (the minimum range is 1 μL) was used to measure the flow rate under different temperatures and confining stresses (Fig. 2). During the experiment, the tip of the volumometer was inhaled into the black ink column, and a closed volume was formed between the end of the core and the

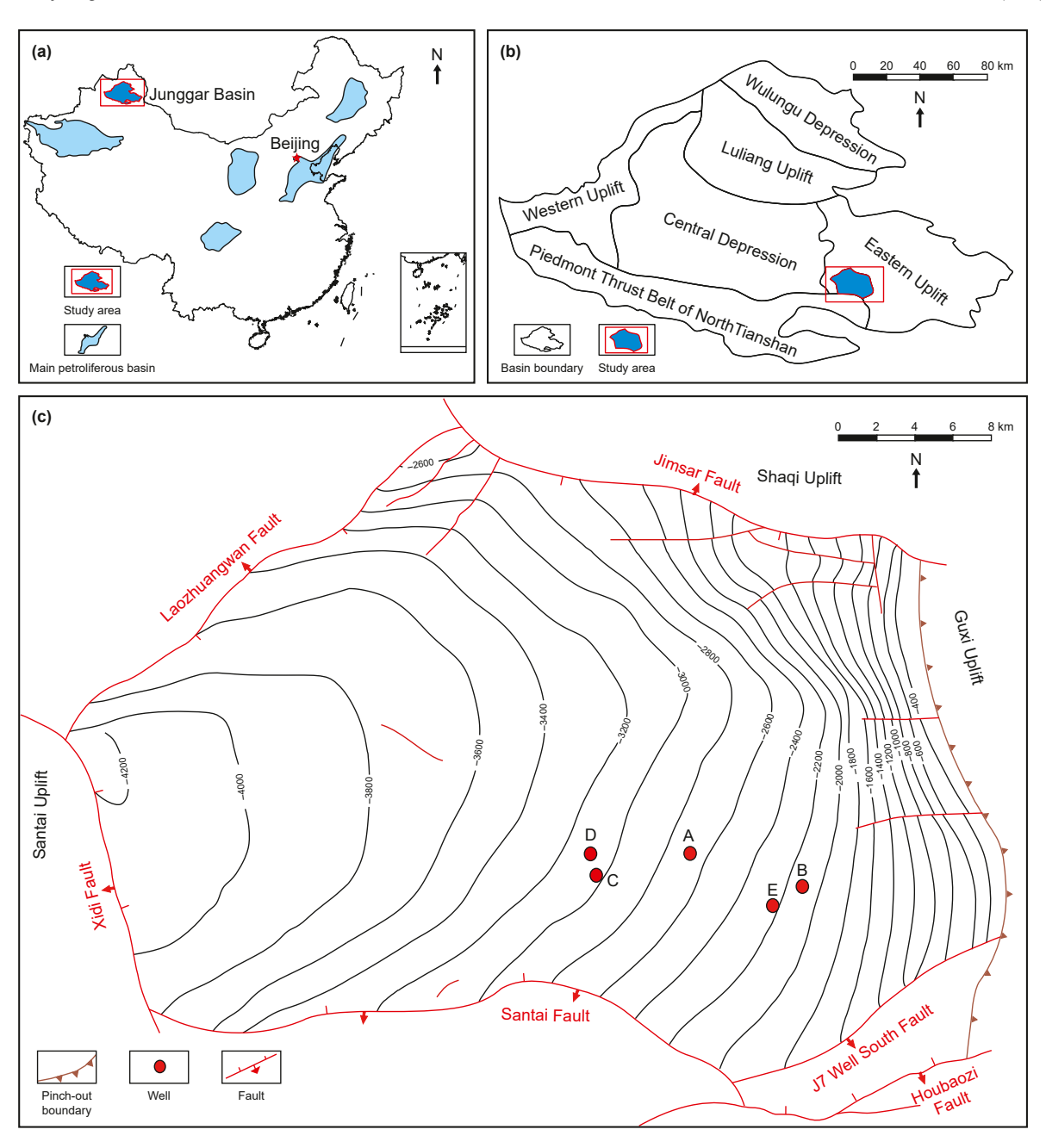


Fig. 1. (a) Location of the Junggar Basin in China. (b) Location of the Jimsar Sag in Junggar Basin (modified from Wang et al., 2019). (c) Tectonic units of the Jimsar Sag and sampling well location (modified from Ding et al., 2023).

Table 1Basic information of samples.

Core ID (No.)	Depth, m	Length, mm	lithology	Porosity, %	Permeability, mD	TOC, %	Quartz, %	K-feldspar, %	Albite, %	Calcite, %	Dolomite, %	Clay, %	Else, %
A-1	3333.94	44.42	Siltstone	15.23	0.0612	2.99	20	7	64.2	0.7	5.1	3	1
A-2	3346.06	27.67	Dolomitic siltstone	15.48	0.095	3.29	18.2	4.8	48	0.3	22.2	4.2	2.3
B-1	2676.86	45.24	Siltstone	13.4	0.0506	3.9	27.3	20.2	21.7	5.5	21.2	4.1	1
C-1	3563.02	46.28	Domomicrite	1.8	0.0046	3.48	16.4	6.6	17.6	0.5	51.8	3.4	3.7
C-2	3642.01	42.66	Dolomitic siltstone	13.78	0.0195	2.98	16.1	6.9	34.8	0.4	37.1	4.2	0.5
D-1	3543.67	34.15	Mudstone	7.47	0.0491	2.34	29	8.7	45.8	10.8	4.1	1.6	1
D-2	3549.53	55.80	Doloarenite	14.61	0.0218	1.05	4.8	1.1	9.4	1	81.8	0.4	2.5
D-3	3693.41	33.04	Siltstone	14.12	0.0253	3.32	15.2	5.7	55.9	0.1	16.6	5.3	1.2
E-1	2769.29	43.55	Siltstone	9.91	0.0101	3.87	26.8	22.2	21.8	5.9	8.6	14.7	1

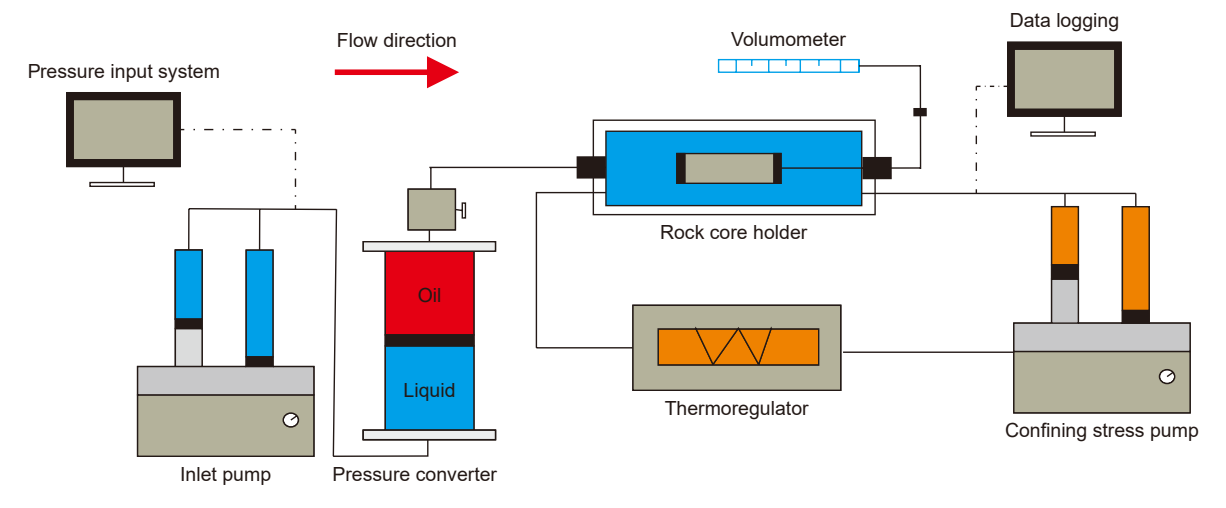


Fig. 2. Flow simulation experiment device (modified from Lin et al., 2022).

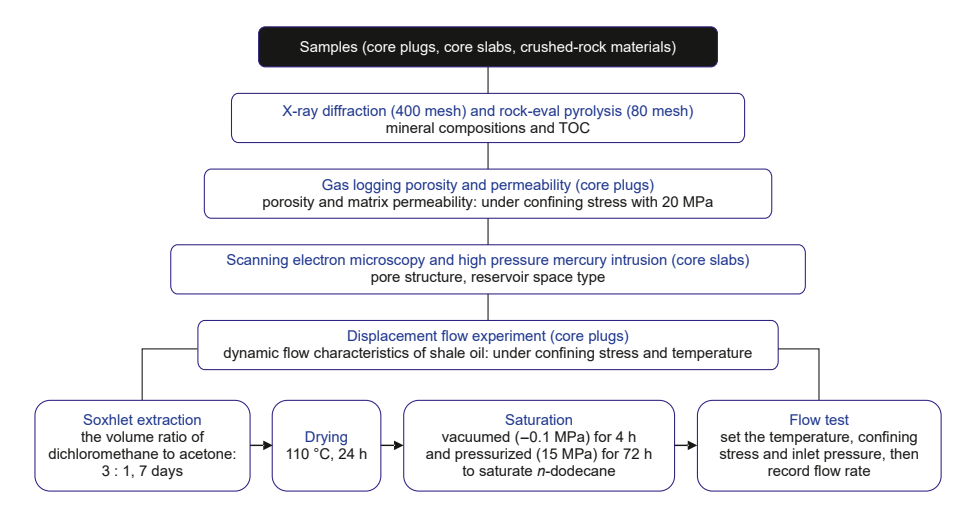


Fig. 3. Workflow of experimental samples.

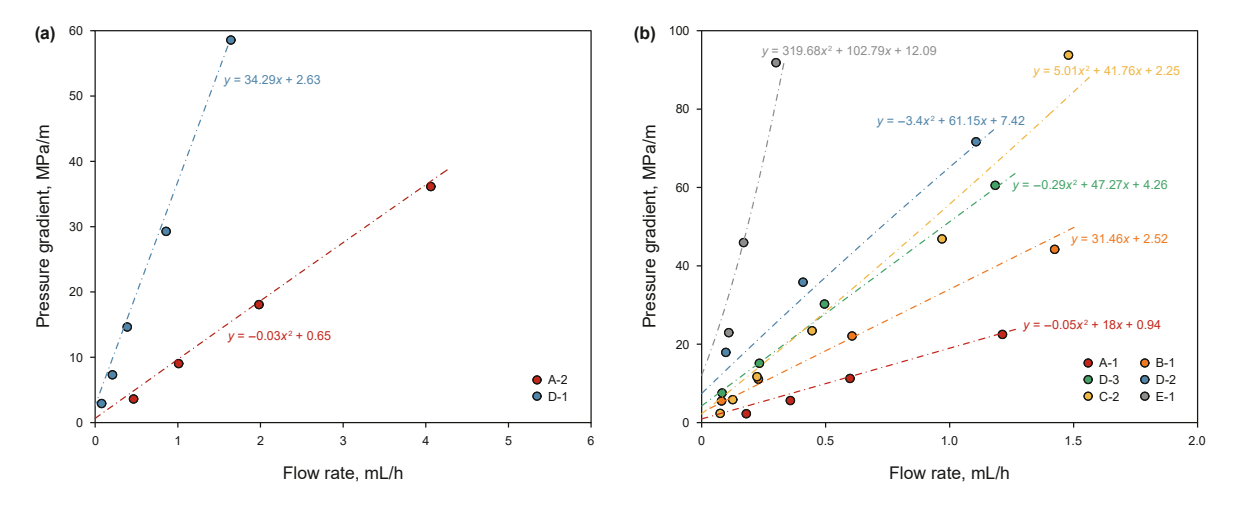


Fig. 4. The fitting curve of TPG in 20 MPa confining stress, 50 °C. (a) High flow rate samples, corresponding to Type I samples in Section 3.1; (b) low flow rate samples, corresponding to Type II samples in Section 3.1.

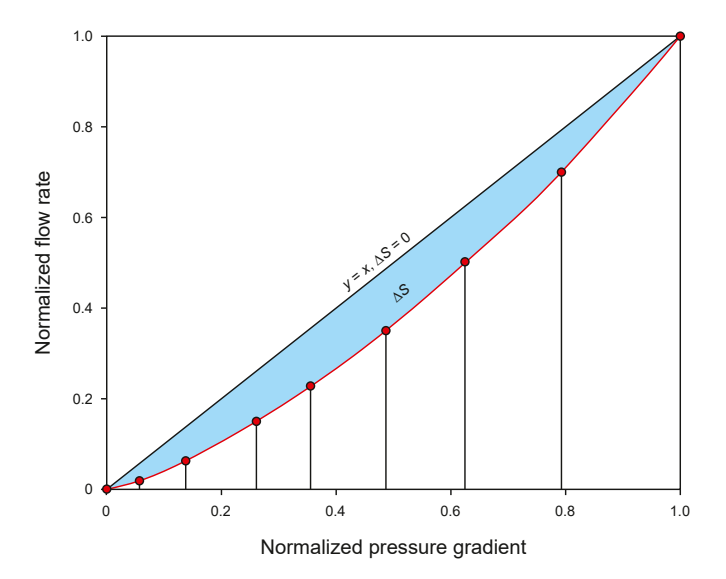


Fig. 5. Total loss of flow rate diagram (modified from Li et al., 2017).

Table 2 Value of MICP parameters.

Core ID (No.)	V _p , cm ³ /g	P _d , MPa	R _{avg} , μm	W _E , %
A-2	0.0827	0.64	0.2048	35.54
D-1	0.038	0.99	0.0649	14.78
B-1	0.0762	2.85	0.0975	31.5
A-1	0.076	2.34	0.1515	32.17
D-3	0.0756	2.91	0.2269	27.83
D-2	0.028	3.62	0.1797	21.3
E-1	0.0529	2.91	0.0494	21.41
C-2	0.0646	2.33	0.1558	26.72
C-1	0.0132	19.98	0.0769	7.03

 $V_{\rm p}$ is the pore volume of the sample; $P_{\rm d}$ is the displacement pressure; $R_{\rm avg}$ is the average throat radius; $W_{\rm E}$ is the mercury withdrawal efficiency reflecting the uniformity of throat distribution.

ink column of the volumometer. When liquid or gas flowed out from the end of the core, the black ink column was pushed. At the same time, the stopwatch accurately recorded the time when the black ink column flowed through a certain volume. Repeated the test and took the stable value as the flow rate.

Qin et al. (2021) performed chromatographic analysis on the crude oil samples of the Lucaogou Formation, in which the main

peak carbon of the P_2l_1 of the Lucaogou Formation was C_{17} , and the main peak carbon of P_2l_2 of the Lucaogou Formation was C_{23} . Considering the loss of light hydrocarbons during sampling and placement, n-dodecane was selected as the simulated oil flow. The viscosity of n-dodecane at 40 °C and 50 °C, determined using Refprop software, measured 1.0595 mPa·s and 0.9178 mPa·s, respectively (Lin et al., 2022). These results demonstrate the viscosity reduction mechanism underlying enhanced shale oil mobility with thermal elevation. The detailed experimental procedure is outlined in Fig. 3.

2.2. Theory and methods

2.2.1. Threshold pressure gradient

The micro-nano pore throats in shale oil reservoirs and the large specific surface area leads to shale oil adsorbing onto the pore walls and forming a boundary layer. It reduces the effective flow space and generates the TPG (Li et al., 2016b). The TPG plays an important role in reservoir production, significantly impacting the determination of optimal injection-production well spacing, optimization of development plans, and enhancement of oil recovery efficiency (Song et al., 2015; Cui et al., 2022). The flow curve

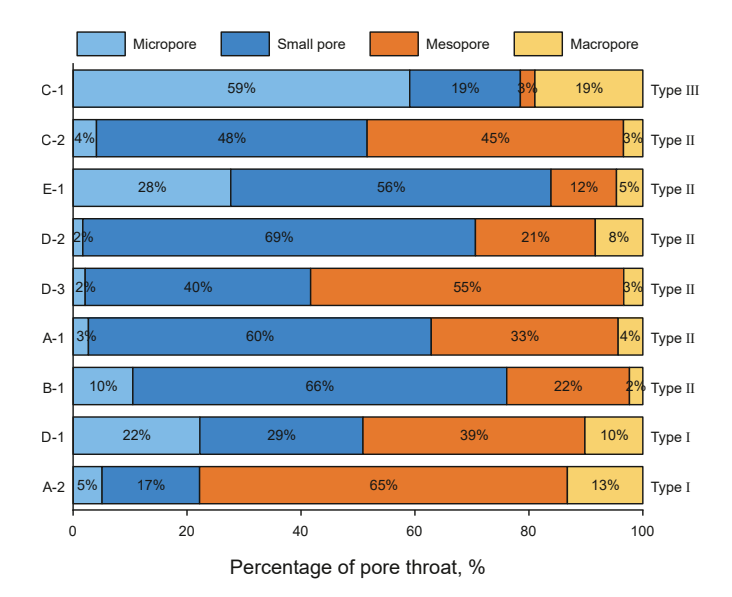


Fig. 7. Pore throat content of different scales.

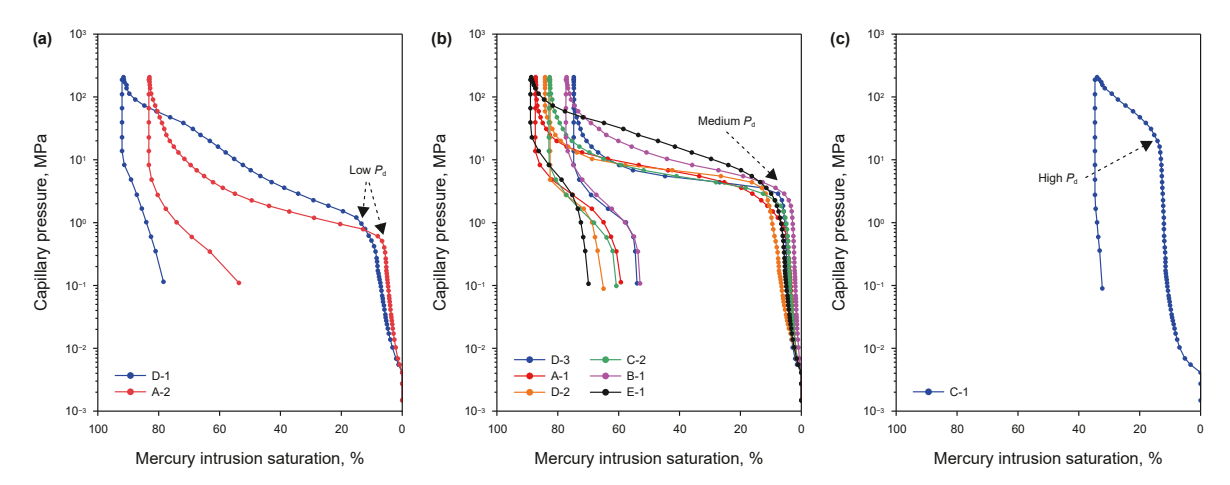


Fig. 6. Mercury intrusion curves of different pore structure types. (a) Type I. (b) Type II. (c) Type III.

depicted by the relationship between pressure gradient and flow rate typically exhibits a parabolic shape, which reflects the nonlinear resistance encountered by the fluid as it flows through the pore throats. To quantify this relationship and estimate the TPG, scholars have proposed the use of quadratic equation fitting methods (Teng et al., 2023). However, as the confining stress increases or the fluid properties change, the flow curve may deviate from the parabolic shape and tend towards linearity.

Consequently, this study employs both quadratic and linear equation fitting approaches to determine the TPG, and uses this parameter to assess flow characteristics (Fig. 4).

2.2.2. Total loss of flow rate

The linear flow theory based on Darcy's law guarantees the successful development of conventional oil reservoirs. However, due to the low permeability of shale reservoirs and the strong

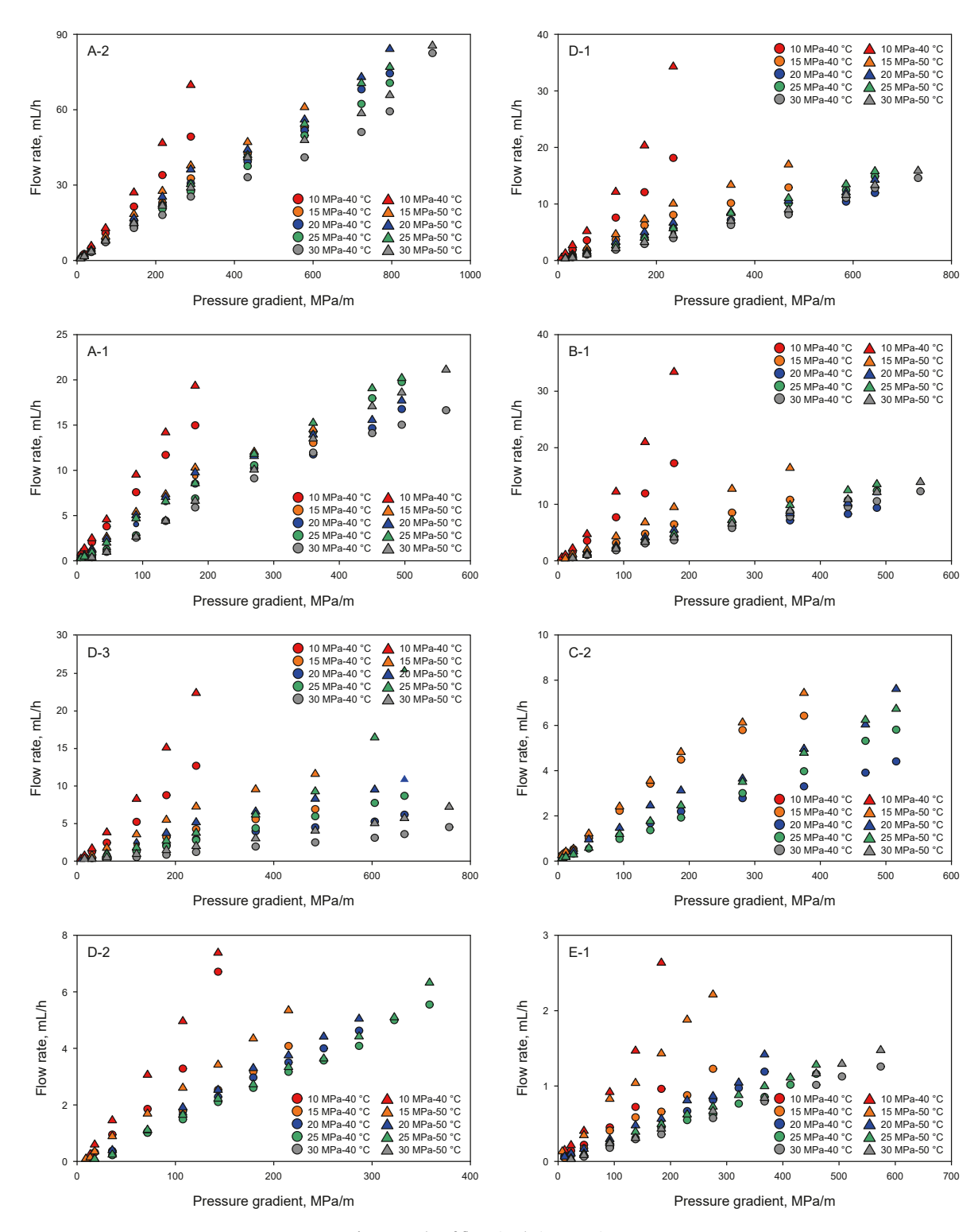


Fig. 8. Results of flow simulation experiment.

interaction between fluid and solid media caused by the large specific surface area of micro-nano pores, the flow of shale oil exhibits nonlinear characteristics, Darcy's law cannot be applied to the development of shale oil reservoirs (Sun et al., 2024). To describe the flow characteristics of shale oil, the ΔS is introduced to quantitatively characterize the degree of deviation from the linear Darcy flow. The value of ΔS ranges from -0.5 to 0.5. When ΔS is equal to 0, the flow characteristics of the fluid conform to Darcy fluid, whereas as the absolute value of ΔS increases, the nonlinear characteristics of the fluid flow become more prominent.

The ΔS is obtained by the area enclosed by the curve connected by the normalized data points measured by the flow experiment and the straight line with a slope of 1 over the origin (Fig. 5). The Min-Max standard deviation calculates the normalized pressure gradient and normalized flow rate. The calculation equation is as follows:

$$y_{i} = \frac{x_{i} - \min_{1 \leq j \leq n} \left\{ x_{j} \right\}}{\max_{1 \leq j \leq n} \left\{ x_{j} \right\} - \min_{1 \leq j \leq n} \left\{ x_{j} \right\}}$$
(1)

$$\Delta S = 0.5 - S \tag{2}$$

where *y* is the normalized data point, dimensionless, and *x* is the experimentally measured flow rate or pressure gradient, mL/h or MPa/m. The *S* is the area enclosed by the curve and the coordinate axis, which can be obtained by integral method.

3. Results and discussion

3.1. Pore structure characteristics

The size, shape, and distribution of pore throats, which are important indicators of pore structure, influence petrophysical parameters as well as reservoir quality and flow capacity (Shi et al., 2023; Li et al., 2024b). The shale oil flow channel is the pore network under the control of pore throats, which has a better matching with the MICP experimental data. Therefore, this study uses MICP test to characterize the pore throat and establishes a pore throat classification scheme suitable for shale reservoirs in the Lucaogou Formation of Jimsar.

According to the Washburn equation, the pore throat size can be obtained from the capillary pressure, and the calculation of pore throat characteristic parameters of the rock sample is

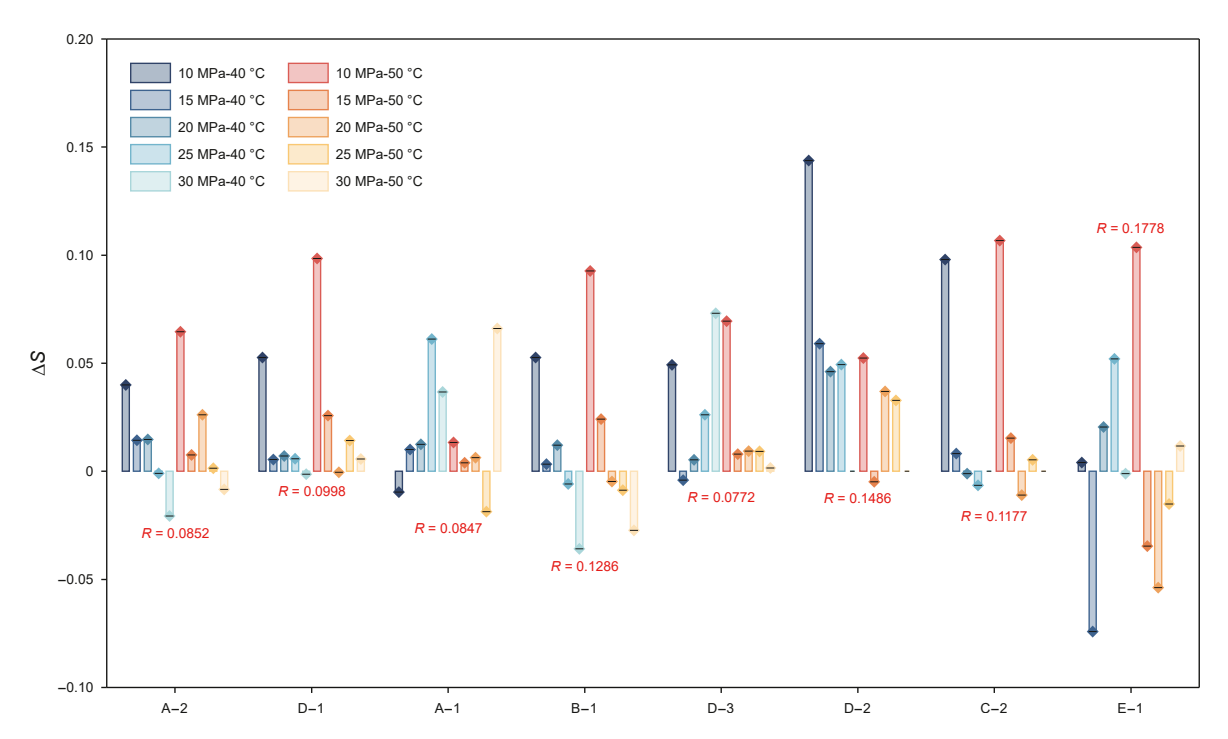


Fig. 9. ΔS under different temperatures and confining stresses.

Table 3The TPG under different experimental conditions.

Core ID (No.)		A-2	D-1	B-1	A-2	D-3	D-2	C-2	E-1		
Confining stress, MPa	Temperature, °C	TPG, MPa	PG, MPa/m								
10	40	0.61	1.04	0.95	0.98	1.26	7.06	1	6.27		
	50	0.24	0.8	0.27	0.63	0.95	3.82	1	3.99		
15	40	0.73	2.49	1.47	1.58	2.76	14.5	2.69	6.54		
	50	0.42	1.47	1.12	0.69	2.42	4.59	2.02	5.04		
20	40	1.14	4.6	3.36	1.87	5.04	15.55	3.2	14.59		
	50	0.65	2.63	2.52	0.94	4.26	7.42	2.25	12.09		
25	40	1.92	6.75	4.35	3.79	8.5	15.74	5.43	21.42		
	50	1.23	5.51	3.57	2.75	3.25	11.55	4.48	20.79		

shown in Table 2 (Washburn, 1921; Rouguerol et al., 2012; Li et al., 2016a). The nine samples were categorized into three groups based on the displacement pressure (Pd): Type I (micron-scale pore throat and low P_d), type II (nano-scale pore throat and medium P_d), and type III (nano-scale pore throat and high $P_{\rm d}$) (Fig. 6). Song et al. (2024) combined the MICP data of shale in limsar with fractal theory and divided pore size into micropore (pore diameter <30 nm), small pore (pore diameter ranges from 30 to 200 nm), mesopore (pore diameter ranges from 200 to 1500 nm) and macropore (pore diameter >1500 nm). This study used this as a standard to count the pore throat content of different scales of experimental samples (Fig. 7). Type I samples mainly feature mesopores, with an average throat radius (R_{avg}) of 0.1349 µm and low P_d (0.82 MPa). The R_{avg} of type II samples (0.134 μm on average) is not much different from that of type I samples, but the $P_{\rm d}$ (2.83 MPa on average) increases obviously. Type III samples have an extremely high number of micropores, with high $P_{\rm d}$ (19.98 MPa) and low mercury injection (34.71%), indicating the poorest pore throat structure.

3.2. Flow characteristics of shale oil

Flow rate describe the flow capacity of the fluid and directly reflects the fluidity of fluid in the porous medium. The flow process of shale oil is dynamic and is influenced by temperature, pore fluid pressure, and pore system (Lin et al., 2022; Du et al., 2023). This study measured the flow rate of samples under different temperatures and confining stresses (Fig. 8). At constant confining stress, the flow rates of nine samples increase with the increasing pressure gradient, and the greater the pressure gradient, the more obvious the increase in flow rate. The flow curves demonstrate a positive correlation between temperature and flow rate, primarily attributed to the decrease in fluid viscosity and concomitant enhancement in fluidity as temperature rises.

However, different samples have different pore throat structure and the degree of flow rate changes with temperature. In addition, the flow rate decreases with the increase of confining stress, but some samples (such as A-2), an increase in confining stress may lead to fracture propagation, increasing the flow rate. Meanwhile, the increase of confining stress weakens the nonlinear

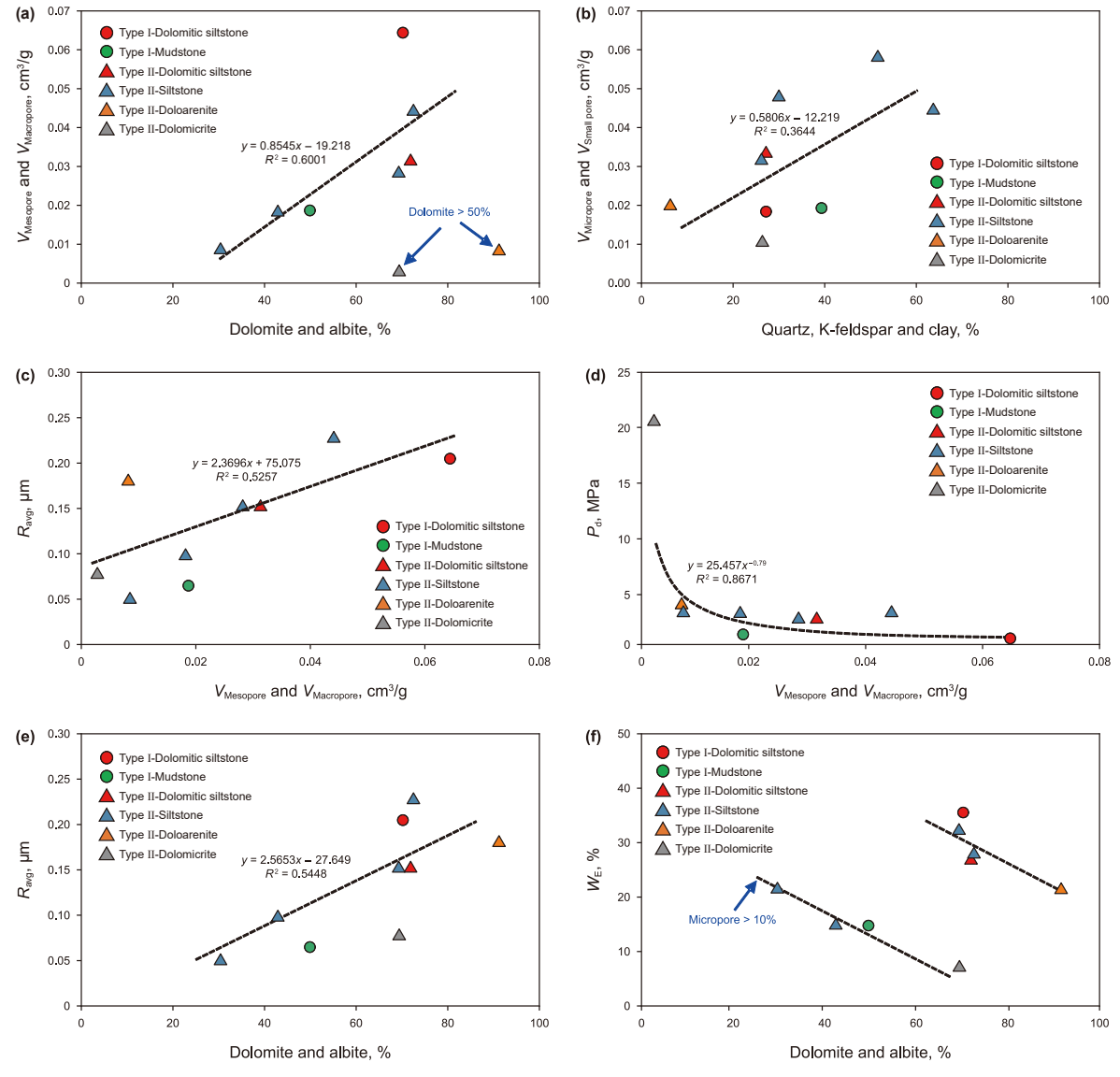


Fig. 10. Coupling relationship between rock composition and pore throat structure.

characteristics of the flow curve. Under the same inlet pressure, the difference in flow rate decreases with the increase of confining stress. Overall, attributed to the low $P_{\rm d}$ and large $R_{\rm avg}$, type I samples display a generally high flow rate. Type II samples have a larger $R_{\rm avg}$ yet a lower flow rate than Type I, but some samples (A-1, B-1, D-3) with good sorting and high pore uniformity have a large flow rate. Type III sample (C-1), characterized by numerous nanoscale pore throats, exhibits a high $P_{\rm d}$, resulting in no flow of n-dodecane.

The ΔS of samples under different temperatures and confining stresses ranging from -0.0742 to 0.1438 (0.0201 on average). The flow characteristics of each sample are influenced to varying degrees by confining stress and temperature, resulting in significant differences in ΔS values under different temperatures and confining stress conditions. But on the whole, ΔS decreases with the increase of confining stress and increases with the increase of temperature (Fig. 9). The pore throat structure characteristics also have a significant effect on the ΔS . The ΔS value of type I reservoir changes less than that of type II reservoir (The average range R for the former is 0.0925, whereas the latter ranges from 0.0772 to 0.1778 with an average of 0.1224. Notably, the ΔS value of E-1 exhibits the most significant fluctuation). Therefore, within type I reservoirs, the fluid-solid interaction is relatively weak, exerting minimal influence on flow, tending towards a linear Darcy flow behavior.

The TPG of 8 samples under various conditions is shown in Table 3. As the confining stress increases, the porosity and permeability of the sample become worse, resulting in a larger TPG. The flow rate rises with temperature, from 40 to 50 $^{\circ}$ C, and the TPG correspondingly lowers. In addition, the TPG also increases with the deterioration of the pore throat structure. In

general, the TPG of shale samples is between 0.24 and 21.42 MPa/m, and the TPG of type I reservoir (0.24–6.75 MPa/m, average value is 2.01 MPa/m) is significantly lower than that of type II reservoir (0.27–21.42 MPa/m, average value is 5.44 MPa/m), demonstrating that the development impact and flow capacity of type I reservoirs are superior to those of type II reservoirs.

3.3. Geological controls of shale oil flow

3.3.1. Coupling of rock composition and pore throat structure analysis

Rock composition is the fundamental factor that determines the pore-throat structure of reservoir spaces, indirectly influencing fluid mobility. The diverse rock compositions subjected to sedimentation and compaction processes form specific pore throat structures, which dictate the flow pathways and efficiency of fluids within the reservoir (Macquaker et al., 2014; Zhang et al., 2022a; Alarji et al., 2022; Li et al., 2024c). Du et al. (2023) investigated the effects of seepage channels formed by different mineral combinations on tight oil flow, found that seepage channels developed by feldspar dissolution pores have better flow conductivity. Research by Song et al. (2024) on the coupling relationship between rock composition and pore throat structure in the Lucaogou Formation of Jimsar has revealed that small pores in the shale oil reservoirs are primarily developed within K-feldspar, quartz, and clay minerals. In contrast, mesopores are mainly derived from interparticle pores of dolomite and albite. Additionally, the degree of development of mesopores and macropores shows a positive correlation with a larger pore diameter and superior reservoir physical properties.

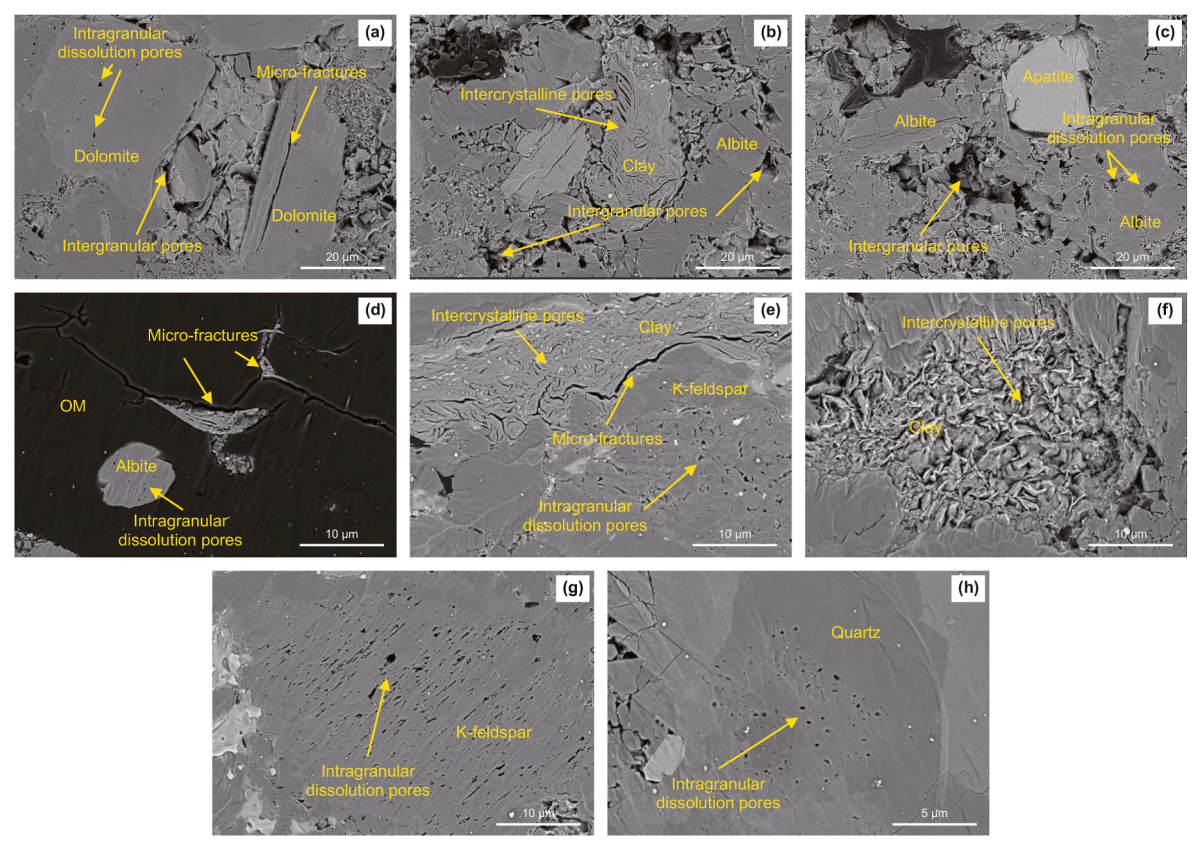


Fig. 11. SEM images of samples. (a) D-3; (b) C-2; (c) B-1; (d) A-2; (e) E-1; (f) C-1; (g) D-1; (f) D-2.

In this study, the combined content of dolomite and albite shows a positive correlation with the total of the mesopore and macropore volume (Fig. 10(a)). In contrast, the total of the micropore and small pore volume are predominantly associated with quartz, K-feldspar and clay (Fig. 10(b)). The development of mesopores and macropores corresponds to larger R_{avg} (Fig. 10(c)), lower P_d (Fig. 10(d)), and improved pore throat structure. The above phenomenons can be observed under SEM images, the carbonate minerals in the Lucaogou Formation are predominantly dolomite. Due to its high compressive strength, dolomite preserves intergranular pores with larger pore sizes. Intragranular dissolution pores and micro-fractures are also observed within the dolomite (Fig. 11(a)). The albite exhibits well-developed residual intergranular pores of large size (Fig. 11(b) and (c)). Additionally, it is often encapsulated by OM in organic-rich samples, with microfractures observable at the contact zones (Fig. 11(d)). The clay mineral content of the experimental samples is low, and most of them are filled between the pores. Due to its strong plasticity and mechanical compaction, the pores are dominated by micropores and small pores (Fig. 11(e) and (f)), and the contribution of microfractures to the flow rate is not obvious under the action of effective stress. Moreover, K-feldspar and quartz mostly develop intragranular dissolution pores, contributing mainly to micropore pore volume and small pore volume (Fig. 11(g) and (h)).

This series of phenomena is consistent with the results of previous study (Song et al., 2024). Therefore, it can be considered that dolomite and albite have a main effect on the pore throat structure (Fig. 10(e) and (f)). However, it is worth noting that when the dolomite content is high (more than 50%), it will form an iron dolomite with the iron element in the fluid and over-cemented, the intergranular pores are reduced, the content of mesopores and macropores is reduced, and the pore throat structure is deteriorated.

3.3.2. Geological control mechanism of shale oil flow

Porosity and permeability are key reservoir factors that influence flow characteristics. Permeability reflects the ability of rock to allow fluid flow under a pressure differential, with higher permeability indicating lower resistance and higher flow rates. Statistical analysis reveals a positive exponential correlation

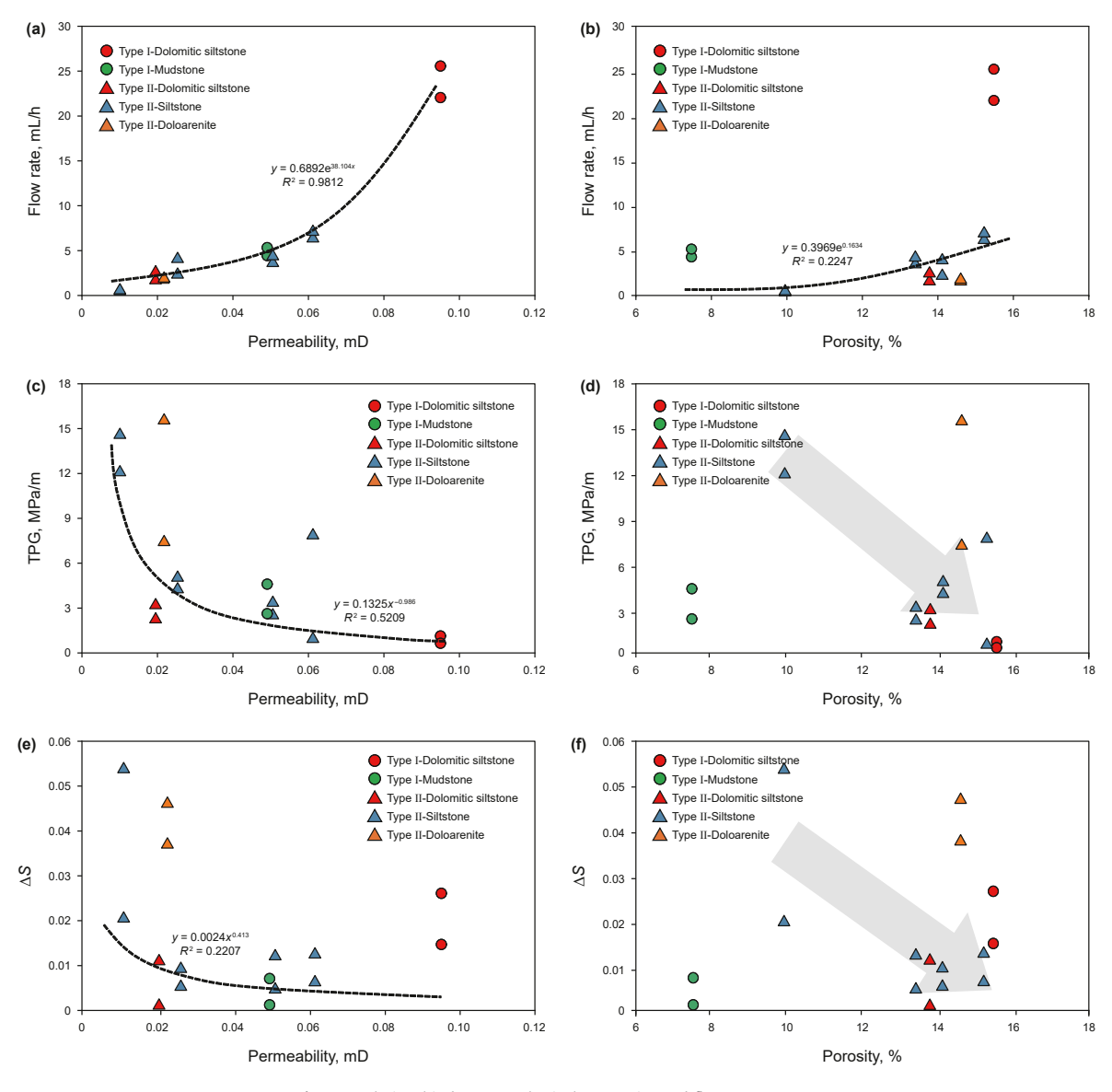


Fig. 12. Relationship between physical properties and flow parameters.

between permeability and flow rate (Fig. 12(a)). The TPG and ΔS have a negative power-law correlation with permeability (Fig. 12 (c)–(e)). However, porosity has a lesser impact on flow compared to permeability. Increased porosity often accompanies improved pore volume, leading to higher flow rates, lower TPG and ΔS (Fig. 12(b)–(d), (f)). The above flow parameters are all taken from the confining stress of 20 MPa. Notably, the mudstone sample (D-1, green circle in Fig. 12) with relatively low porosity shows high flow rates, and low TPG and ΔS . This is due to the fact that shale oil flow occurs mainly in interconnected mesopores and macropores, and the relatively high macropores content, low $P_{\rm d}$, and superior connectivity lead to the good flow characteristics of this sample.

The relationship between reservoir physical properties and flow characteristics indicates that permeability plays a controlling role in shale oil flow. The controlling effect of pore throat structure on permeability has been confirmed by numerous studies (Lala and El-Sayed, 2017; Yin et al., 2020; Wang et al., 2024). To elucidate the micro-control mechanisms of shale oil flow, we investigated the relationship between pore throat structure and permeability. The results show that permeability is primarily controlled by mesopores and macropores, with more developed mesopores and macropores leading to a larger R_{avg} and lower P_d , thereby enhancing shale oil flow capacity (Fig. 13). Additionally, samples with high connectivity (higher ratio of permeability to porosity, higher reservoir quality index, reflecting stronger reservoir connectivity) have lower R_{avg} , but still exhibit higher permeability (Fig. 13(c)), further emphasizing the controlling effect of pore throat structure on shale oil flow.

The coupling relationship between rock composition and pore throat structure indicates that K-feldspar and quartz primarily feature micropores and small pores formed by dissolution, with complex pore morphology. Clay exhibit smaller particle sizes and are arranged in ribbon-like structures, resulting in poor pore throat structure. In contrast, dolomite and albite predominantly

feature intergranular pores with regular pore morphology and better pore throat structure, serving as primary pathways for shale oil flow. However, excessive dolomite content can degrade pore throat connectivity due to ferroan dolomitic cementation. Additionally, the relationship between pore throat structure and shale oil flow parameters reveals that samples with well-developed mesopores and macropores, better connectivity, and lower $P_{\rm d}$ have a controlling effect on shale oil flow. Therefore, the coupled relationship between rock composition and pore throat structure synergistically controls shale oil flow.

3.4. Quantitative evaluation on the shale oil flow

Nonlinear flow characteristics, flow rate and TPG in low-permeability reservoirs significantly impact reservoir development and productivity (Dong et al., 2019; Zhu et al., 2022; Yue et al., 2024). Analysis of parameter relationships reveals a weak negative power-law correlation between ΔS and flow rate (Fig. 14 (a)). Flow rate demonstrates a relatively strong negative correlation with TPG (Fig. 14(b)), while ΔS exhibits a moderate linear positive correlation with TPG (Fig. 14(c)). Consequently, samples with lower TPG generally exhibit higher flow rate. These findings indicate that flow characteristics can be assessed judged according to the ΔS and flow rate or ΔS and TPG.

The flow evaluation chart of shale oil in the Lucaogou Formation of Jimsar is constructed based on flow rate and $\Delta S \times 100$ under different conditions (Fig. 15). Based on frequency distribution, the flow rates and ΔS are categorized into three intervals. Optimal flow characteristics are observed when the flow rate exceeded 8.5 mL/h and the absolute $\Delta S \times 100$ is below 0.85. Conversely, the worst flow characteristics occur at flow rates below 3.6 mL/h with an absolute $\Delta S \times 100$ exceeding 3.6. Therefore, the ratio of ΔS to flow rate effectively reflects the quality of flow characteristics. By utilizing slope values of k=0.1 and 1, the evaluation chart can be

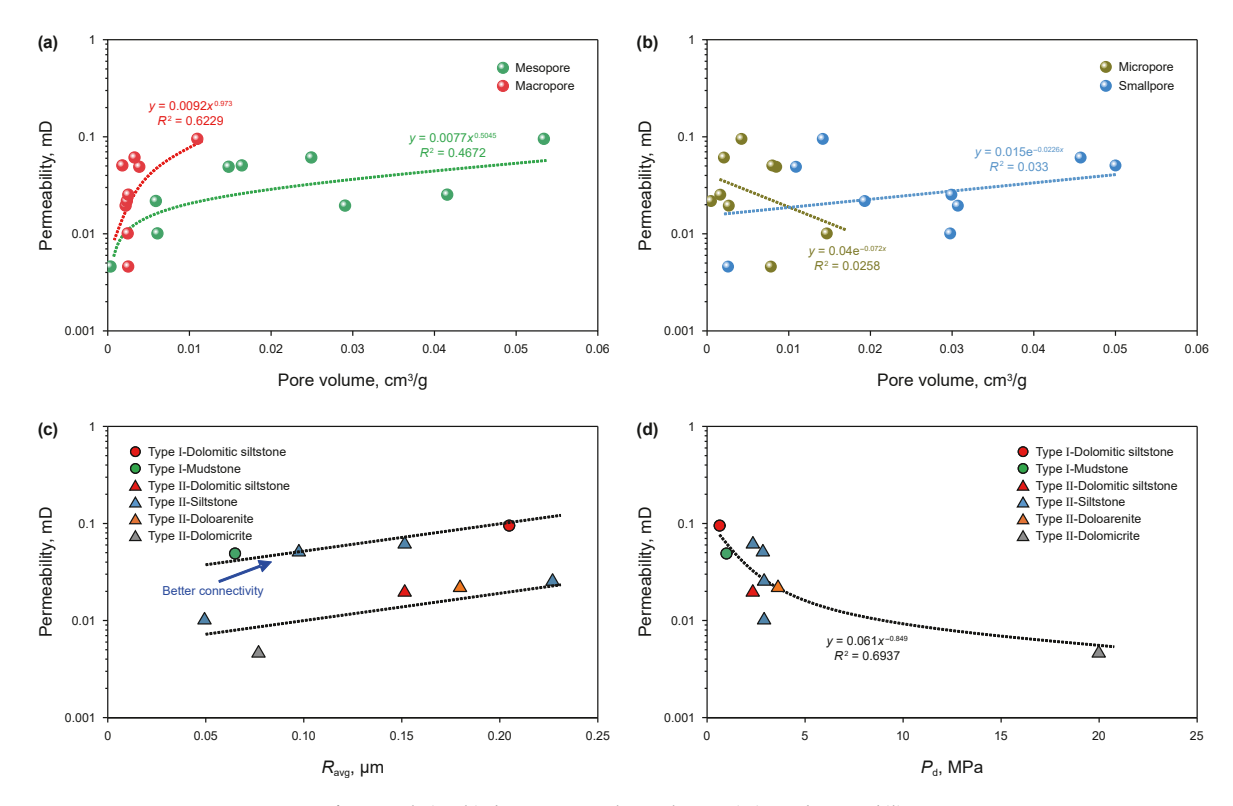
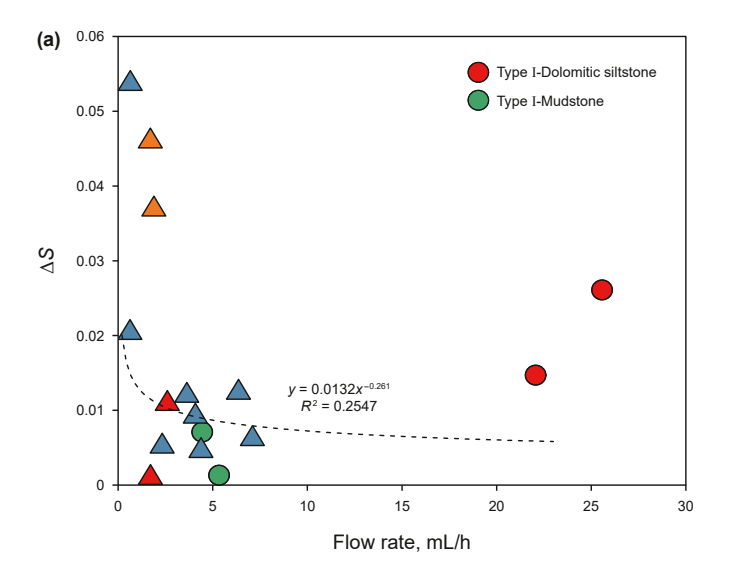
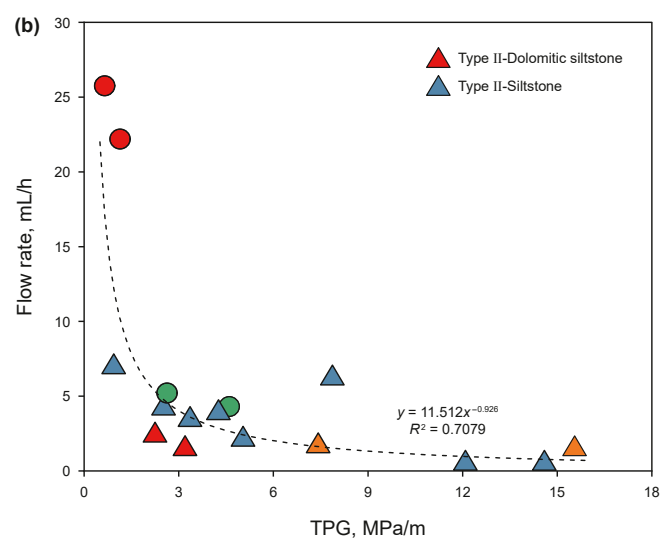


Fig. 13. Relationship between pore throat characteristics and permeability.





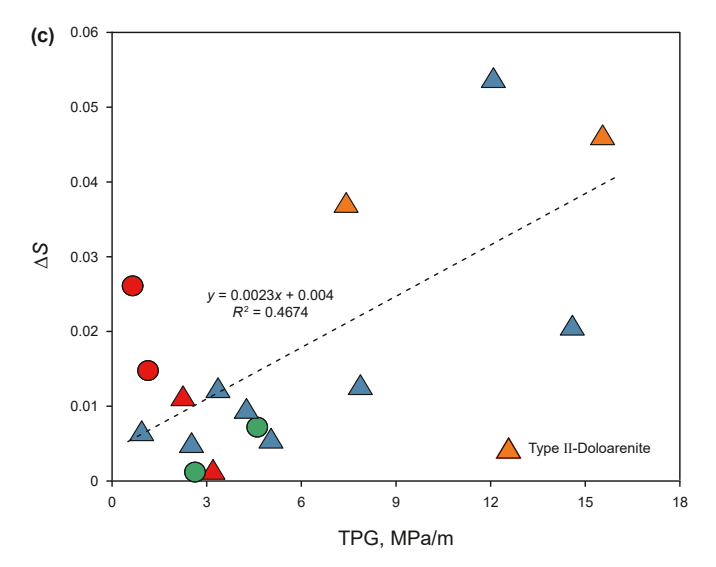


Fig. 14. The relationship between flow parameters.

divided into three distinct zones, superior flow zone, transitional flow zone and poor flow zone. The chart indicates that Type I samples, based on pore throat structure, exhibit significantly

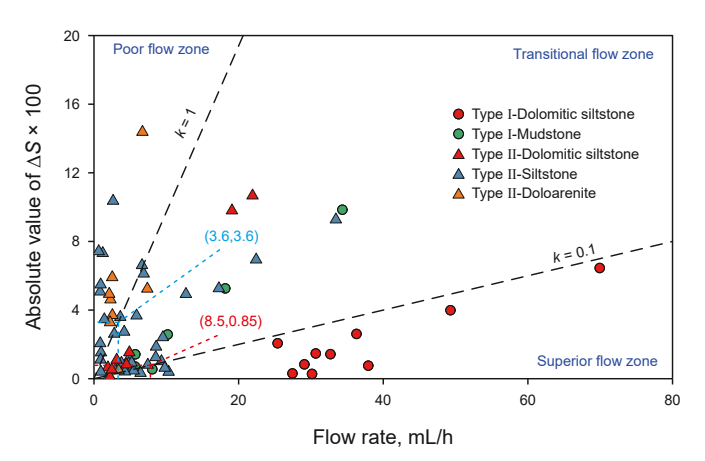


Fig. 15. Evaluation chart for the flow of shale oil in the Lucaogou Formation of Jimsar.

superior flow characteristics compared to those of Type II. Additionally, different lithological samples display distinct flow behaviors. Among Type I samples, dolomitic siltstone shows markedly better flow characteristics than mudstone. Similarly, in Type II samples, dolomitic siltstone also demonstrates good flow properties, confirming the controlling effect of dolomite and albite on pore throat structure and, consequently, on flow. However, when the dolomite content is excessively high, the pore throat structure deteriorates, resulting in poorer flow characteristics for doloarenite and dolomicrite.

3.5. Favorable reservoir characteristics of shale oil flow

The research on the flow control mechanism of shale oil indicates that both rock composition and pore throat structure collaboratively regulate shale oil flow. The rock composition-pore throat structure-shale oil flow model corresponds to four categories of samples: large pores with large throats, large pores with small throats, small uniform pores with throats, and small complex pores with throats (Fig. 16). Fig. 16(a) depicts the rock composition and pore throat structure of sample A-2, which features well-developed dolomite and albite, intergranular pores, a high content of mesopores and macropores, low P_d , and strong shale oil flow capability (indicated by more red arrows for stronger flow capability). Fig. 16(b) represents sample C-2 with large pores but small throats, similar in rock composition to A-2 but with inferior pore throat structure, resulting in poorer flow capability due to its fine throats. Fig. 16(c) shows mudstone sample D-1, with lower porosity but evenly distributed pore throat structure and good pore connectivity, thus exhibiting favorable flow capability. Fig. 16(d) illustrates sample C-1 with the worst physical properties, excessive dolomite development, dense reservoir, complex flow paths, and no detected flow rate during physical simulation experiments.

Wells C and D, situated in adjacent locations with similar geological conditions, are both straight wells without hydraulic fracturing treatment. Consequently, the reservoir flow characteristics can reflect the well yield. Excluding engineering factors, production data reveal that after 230 days of operation, the daily oil yield of Well C plummeted dramatically, with its total oil yield being significantly lower than that of Well D (Fig. 17). This consistency with the low flow rate observed in physical simulation experiments using Well C samples further verifies the synergistic control of compositional characteristics and pore throat structure on shale oil flow. In conclusion, samples with well-developed dolomite and albite, typically represented by dolomitic siltstone

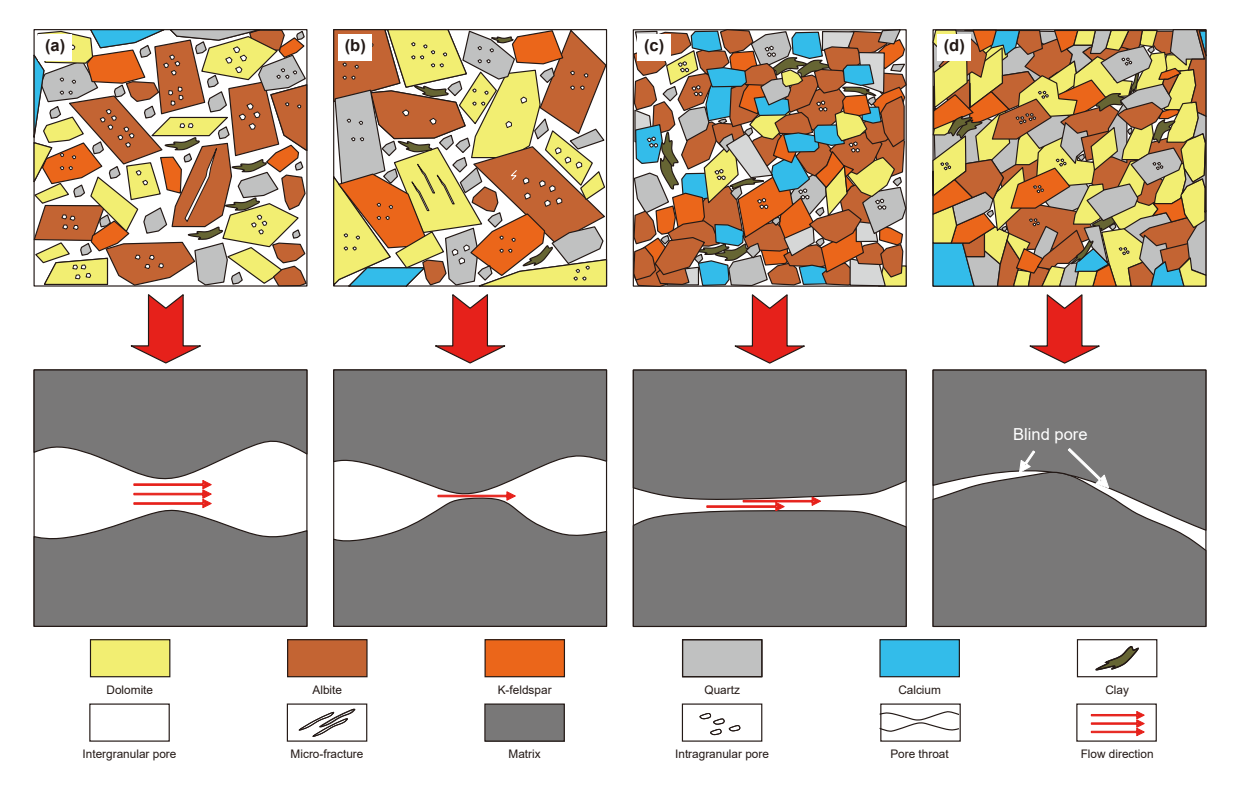


Fig. 16. Rock composition-pore throat structure-shale oil flow pattern diagram.

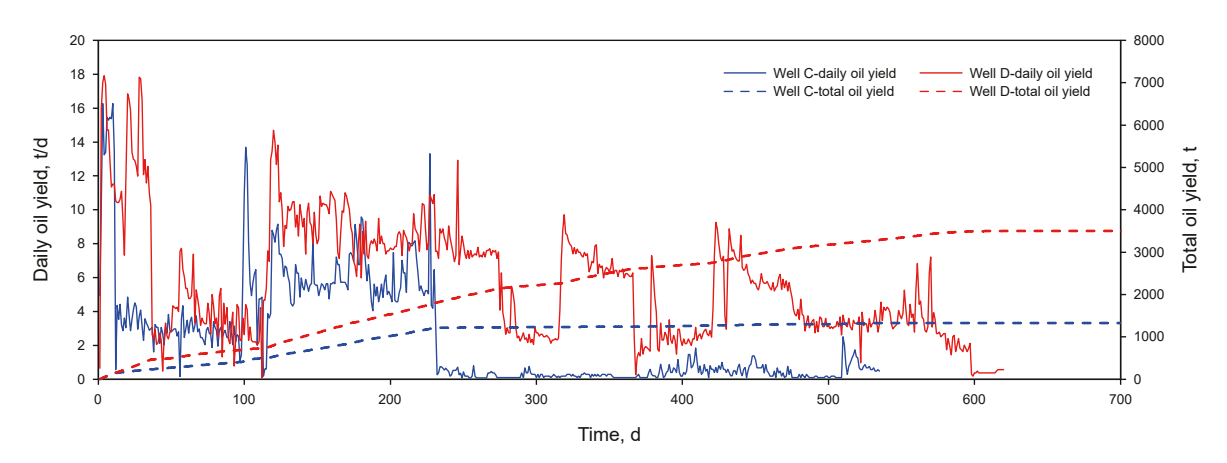


Fig. 17. Oil production curves of Wells C and D.

lithology, exhibit stronger shale oil flow capability as their pore throat structures become more developed. Therefore, during the development phase, for dolomitic siltstone characterized by well-developed mesopores and macropores, emphasis should be placed on preserving and enhancing pore connectivity to avoid disrupting pore structures that may impact productivity. Conversely, for potential reservoirs dominated by micropores, horizontal well technology combined with fracturing can be employed to modify the reservoir, adjust pore distribution and structure, and optimize pore connectivity, thereby improving fluid mobility and achieving high and stable shale oil production.

4. Conclusions

(1) The MICP experiment classified the samples into three categories: micron-scale pore throats with low P_d , nanoscale pore throats with medium P_d , and nano-scale pore

- throats with high $P_{\rm d}$. Most of the experimental samples exhibited type II pore throat structures with nano-scale pore throats and medium $P_{\rm d}$. SEM revealed that the studied samples primarily developed dissolution pores and intercrystalline pores, with a low degree of organic matter pore development and visible micro-fractures development.
- (2) The results of the flow simulation experiments demonstrated that the flow rate of the samples increased with the increase in pressure gradient, and the higher the confining stress, the smaller the flow rate. The ΔS of most samples decreases with the increase of confining stress and increases with the increase of temperature. Conversely, the TPG increased with the increase in confining stress and decreased with the temperature rise.
- (3) Rock composition and pore throat structure synergistically control the flow of shale oil. Mesopores and macropores are

- mostly developed between dolomite or albite. Dolomite and albite development correlates with enhanced mesopores and macropores, leading to improved pore throat structure, larger R_{avg} , lower P_{d} , and superior shale oil fluidity.
- (4) The flow evaluation chart based on flow parameters indicates that type I samples exhibit significantly better flow characteristics than type II samples, with dolomitic siltstone showing superior flow properties compared to other lithologies. Additionally, ignoring the influence of engineering factors, the flow physical simulation results and production data further confirm this view.

CRediT authorship contribution statement

Jia-Qi Liu: Formal analysis, Investigation, Writing – original draft. **Jun-Qian Li:** Supervision, Validation, Writing – review & editing. **Zhao-Jing Song:** Methodology, Project administration. **An-Chao Shen:** Conceptualization, Data curation.

Declaration of competing interest

The authors declare that they have no known competing financial interests or personal relationships that could have appeared to influence the work reported in this paper.

Acknowledgments

This work was financially supported by the National Natural Science Foundation of China (No. 41972123), and the Support Plan for Outstanding Youth Innovation Team in Shandong Higher Education Institutions (No. 2022KJ060). We thanks to the Exploration and Development Research Institute of Xinjiang Oilfield for providing shale core samples.

Acronyms

TPG Threshold pressure gradient ΔS Total loss of flow rate

MICP Mercury injection capillary pressure

SEM Scanning electron microscopy

OM Organic matter
TOC Total organic carbon

 $V_{\rm p}$ Volume pore $V_{\rm Micropore}$ Micropore volume $V_{\rm Small pore}$ Small pore volume $V_{\rm Mesopore}$ Mesopore volume $V_{\rm Macropore}$ Macropore volume $P_{\rm d}$ Displacement pressure $R_{\rm avg}$ Average pore throat radius $W_{\rm E}$ Mercury withdrawal efficiency

R Range

References

- Alarji, H., Clark, S., Regenauer-Lieb, K., 2022. Wormholes effect in carbonate acid enhanced oil recovery methods. Adv. Geo-Energy Res. 6 (6), 492–501. https:// doi.org/10.46690/ager.2022.06.06.
- Bai, L.H., Liu, B., Du, Y.J., et al., 2022. Distribution characteristics and oil mobility thresholds in lacustrine shale reservoir: insights from N₂ adsorption experiments on samples prior to and following hydrocarbon extraction. Pet. Sci. 19 (2), 486–497. https://doi.org/10.1016/j.petsci.2021.10.018.
- Barenblatt, G.I., Zheltov, I.P., Kochina, I.N., 1960. Basic concepts in the theory of seepage of homogeneous liquids in fissured rocks. J. Appl. Math. Mech. 24 (5), 852–864. https://doi.org/10.1016/0021-8928(60)90107-6.
- Cui, C.Z., Zhang, W.Q., Zhu, Y.W., et al., 2022. Method for determining limit well spacing of chemical flooding after reservoir steam soak in heavy oil reservoir.

J. Univ. Petrol., China. 46 (1), 97–103. https://doi.org/10.3969/j.issn.1673-5005.2022.01.011 (in Chinese).

- Dang, W., Zhang, J.C., Nie, H.K., et al., 2022. Microscopic occurrence characteristics of shale oil and their main controlling factors: a case study of the 3rd submember continental shale of Member 7 of Yanchang Formation in Yan'an area, Ordos Basin. Acta Petrol. Sin. 43 (4), 507–523. https://doi.org/10.7623/ syxb202204005 (in Chinese).
- Ding, X.J., He, W.J., Liu, H.L., et al., 2023. Organic matter accumulation in lacustrine shale of the Permian Jimsar Sag, Junggar Basin, NW China. Pet. Sci. 20 (3), 1327–1346. https://doi.org/10.1016/j.petsci.2022.11.004.
 Dong, M.D., Yue, X.A., Shi, X.D., et al., 2019. Effect of dynamic pseudo threshold
- Dong, M.D., Yue, X.A., Shi, X.D., et al., 2019. Effect of dynamic pseudo threshold pressure gradient on well production performance in low-permeability and tight oil reservoirs. J. Petrol. Sci. Eng. 173, 69–76. https://doi.org/10.1016/j. petrol.2018.09.096.
- Du, S.H., Jin, J., Shi, Y.M., et al., 2023. Complex flow in tight oil reservoirs: A new perspective. Mar. Petrol. Geol. 150, 106095. https://doi.org/10.1016/j. marpetgeo.2023.106095.
- Hou, Y.C., Wang, F.R., He, S., et al., 2017. The properties and shale oil potential of saline lacustrine shales in the Qianjiang Depression, Jianghan Basin. China. Mar. Petrol. Geol. 86, 1173–1190. https://doi.org/10.1016/j.marpetgeo.2017.07.008.
- Jia, L.L., Zhong, L.G., Li, S.H., et al., 2024. Study of the liquid resistance effect of water-in-oil emulsions in porous media. Pet. Sci. 21 (6), 4165–4175. https://doi. org/10.1016/j.petsci.2024.07.019.
- Jin, Z.J., 2023. Hydrocarbon accumulation and resources evaluation: recent advances and current challenges. Adv. Geo-Energy Res. 8 (1), 1-4. https://doi.org/10.46690/ager.2023.04.01.
- Lala, A.M.S., El-Sayed, N.A., 2017. Controls of pore throat radius distribution on permeability. J. Petrol. Sci. Eng. 157, 941–950. https://doi.org/10.1016/j.petrol.2017.08.005.
- Li, D.L., Zha, W.S., Liu, S.F., et al., 2016b. Pressure transient analysis of low permeability reservoir with pseudo threshold pressure gradient. J. Petrol. Sci. Eng. 147, 308–316. https://doi.org/10.1016/j.petrol.2016.05.036.
- Li, J.Q., Lu, S.F., Cai, Y.D., et al., 2017. Impact of coal ranks on dynamic gas flow: an experimental investigation. Fuel 194, 17–26. https://doi.org/10.1016/j.fuel.2016.12.079.
- Li, J.Q., Cai, J.C., 2023. Quantitative characterization of fluid occurrence in shale reservoirs. Adv. Geo-Energy Res. 9 (3), 146–151. https://doi.org/10.46690/ ager 2023 09 02
- Li, J.Q., Song, Z.J., Wang, M., et al., 2024a. Quantitative characterization of microscopic occurrence and mobility of oil in shale matrix pores: A case study of the Shahejie Formation in the Dongying Sag. Petrol. Sci. Bull. 9 (1), 1–20. https://doi.org/10.3969/j.issn.2096-1693.2024.01.001 (in Chinese).
- Li, J.Q., Wang, Y.S., Song, Z.J., et al., 2024b. Mobility of connate pore water in gas shales: a quantitative evaluation on the Longmaxi shales in the southern Sichuan Basin. China. Mar. Petrol. Geol. 161, 106674. https://doi.org/10.1016/j.marpetgeo.2023.106674.
- Li, J.Q., Yang, X.D., Wang, M., et al., 2024c. Quantum physisorption behavior of methane in nanoporous shales: Model and new mechanism. Mar. Petrol. Geol. 170, 107129. https://doi.org/10.1016/j.marpetgeo.2024.107129.
- Li, L., Hao, Y.M., Lyu, Y.T., et al., 2020. Experimental investigation on low-velocity seepage characteristics and influencing factors in a shale oil reservoir. J. Petrol. Sci. Eng. 195, 107732. https://doi.org/10.1016/j.petrol.2020.107732.
- Li, L.K., Wang, S., Jia, W.J., et al., 2022. Mathematical model of shale oil seepage at micro-nano pore scale. Energies 15 (21), 8041. https://doi.org/10.3390/ en15218041.
- Li, Z.Q., Oyediran, I.A., Huang, R.Q., et al., 2016a. Study on pore structure characteristics of marine and continental shale in China. J. Nat. Gas Sci. Eng. 33, 143–152. https://doi.org/10.1016/j.jngse.2016.05.011.
- Lin, Z.Z., Li, J.Q., Wang, M., et al., 2022. Organic fluid migration in low permeability reservoirs restricted by pore structure parameters. J. Petrol. Sci. Eng. 218, 111028. https://doi.org/10.1016/j.petrol.2022.111028.
- Lin, Z.Z., Li, J.Q., Lu, S.F., et al., 2023. The occurrence characteristics of oil in shales matrix from organic geochemical screening data and pore structure properties: An experimental study. Pet. Sci. 21, 1–13. https://doi.org/10.1016/j. petsci.2023.09.002.
- Liu, J., Yang, Y.F., Sun, S.Y., et al., 2022. Flow behaviors of shale oil in kerogen slit by molecular dynamics simulation. Chem. Eng. Sci. 434, 134682. https://doi.org/ 10.1016/j.cej.2022.134682.
- Macquaker, J.H.S., Taylor, K.G., Keller, M., et al., 2014. Compositional controls on early diagenetic pathways in fine-grained sedimentary rocks: implications for predicting unconventional reservoir attributes of mudstones. AAPG Bull. 93, 587–603. https://doi.org/10.1306/08201311176.
- Qin, J.H., Gao, X.B., Peng, S.C., et al., 2021. Geochemical characteristics and oilsource correlation of shale oil in Jimsar Sag, Junggar Basin. China. J. Univ. Petrol., Northeast 45 (1), 1–10. https://doi.org/10.3969/j.issn.2095-4107.2021.01.001 (in Chinese).
- Rouquerol, J., Baron, G.V., Denoyel, R., et al., 2012. The characterization of macroporous solids: an overview of the methodology. Microporous Mesoporous Mater. 154, 2–6. https://doi.org/10.1016/j.micromeso.2011.09.031.
- Shi, K.Y., Pang, X.Q., Chen, J.Q., et al., 2023. Pore structure characteristics and evaluation of carbonate reservoir: a case study of the lower carboniferous in the Marsel exploration area, Chu-Sarysu Basin. Nat. Resour. Res. 32, 771–793. https://doi.org/10.1007/s11053-023-10166-8.
- Song, H.Q., Cao, Y., Yu, M.X., et al., 2015. Impact of permeability heterogeneity on production characteristics in water-bearing tight gas reservoirs with threshold

pressure gradient. J. Nat. Gas Sci. Eng. 22, 172–181. https://doi.org/10.1016/j.ingse.2014.11.028.

- Song, Z.J., Li, J.Q., Sun, L.H., et al., 2024. Control of physical properties by the matching between rock components and pore structure in shale reservoirs of the Permian Lucaogou Formation, Jimusar Sag. Energy Fuel. 38, 12938–12948. https://doi.org/10.1021/acs.energyfuels.4c02012.
- Sun, M.D., Fu, J.J., Wang, Q.M., et al., 2024. Pore network characterization and fluid occurrence of shale reservoirs: state-of-the-art and future perspectives. Adv. Geo-Energy Res. 12 (3), 161–167. https://doi.org/10.46690/ager.2024.06.01.
- Sun, S., Liang, S., Liu, Y.K., et al., 2023. A review on shale oil and gas characteristics and molecular dynamics simulation for the fluid behavior in shale pore. J. Mol. Liq. 376, 121507, https://doi.org/10.1016/j.molliq.2023.121507.
- Teng, Y.T., Wang, Y.F., Li, Z.H., et al., 2023. Temperature effect on non-Darcian flow in low-permeability porous media. J. Hydrol. 616, 128780. https://doi.org/10.1016/j.jhydrol.2022.128780.
- Wang, H., Cai, J.C., Su, Y.L., et al., 2023. Imbibition behaviors in shale nanoporous media from pore-scale perspectives. Capi 9 (2), 32–44. https://doi.org/ 10.46690/capi.2023.11.02.
- Wang, J., Cao, Y.C., Liu, K.Y., et al., 2019. Fractal characteristics of the pore structures of fine-grained, mixed sedimentary rocks from the Jimsar Sag, Junggar Basin: Implications for lacustrine tight oil accumulations. J. Petrol. Sci. Eng. 182, 106363. https://doi.org/10.1016/j.petrol.2019.106363.
- Wang, X.D., Zhang, Q., Xu, J.L., et al., 2024. Hydrodynamic resistance of pore-throat structures and its effect on shale oil apparent permeability. J. Coal Sci. Tec. 11, 22. https://doi.org/10.1007/s40789-024-00671-3.
- Wang, X.K., Sheng, J.J., 2017. Effect of low-velocity non-Darcy flow on well production performance in shale and tight oil reservoirs. Fuel 190, 41–46. https://doi.org/10.1016/j.fuel.2016.11.040.
- Wang, X.J., Song, Y., Guo, X.G., et al., 2022. Pore-throat structure characteristics of tight reservoirs of the Middle Permian Lucaogou Formation in the Jimsar sag, Junggar Basin, Northwest China. J. Petrol. Sci. Eng. 208, 109245. https://doi.org/ 10.1016/j.petrol.2021.109245.
- Washburn, E.W., 1921. The dynamics of capillary flow. Phys. Rev. 17 (3), 273–283. https://doi.org/10.1103/physrev.17.273.
- Yang, W., Wang, Y.H., Xie, M., et al., 2023. Effect of lithofacies on differential movable fluid behaviors of saline lacustrine fine-grained mixed sedimentary sequences in the Jimusar sag, Junggar Basin, NW China: Forcing mechanisms and multi-scale models. Mar. Petrol. Geol. 150, 106150. https://doi.org/10.1016/ j.marpetgeo.2023.106150.
- Yang, Z., Zou, C.N., Hou, L.H., et al., 2019. Division of fine-grained rocks and selection of "sweet sections" in the oldest continental shale in China: Taking the

- coexisting combination of tight and shale oil in the Permian Junggar Basin. Mar. Petrol. Geol. 109, 339–348. https://doi.org/10.1016/j.marpetgeo.2019.06.010.
- Yin, X.D., Jiang, S., Chen, S.J., et al., 2020. Impact of rock type on the pore throat structures and physical properties within a tight sandstone reservoir in the Ordos Basin, NW China. Pet. Sci. 17, 896–911. https://doi.org/10.1007/s12182-020-0466.y.
- Yu, Y.J., Wang, H.Y., Liu, D.X., et al., 2023. Development status and feasibility evaluation index system of continental shale oil demonstration area in China. Earth Sci. 48 (1), 191–205. https://doi.org/10.3799/dqkx.2022.422.
- Yue, M., Zhu, W.Y., Gou, F.F., et al., 2024. Impacts of proppant distribution on development of tight oil reservoirs with threshold pressure gradient. Pet. Sci. 21, 445–457. https://doi.org/10.1016/j.petsci.2023.08.030.
- Zhang, J.Y., Liu, G.D., Cao, Z., et al., 2019. Characteristics and formation mechanism of multi-source mixed sedimentary rocks in a saline lake, a case study of the Permian Lucaogou Formation in the Jimusaer Sag, Northwest China. Mar. Petrol. Cept. 102, 704, 724, https://doi.org/10.1016/j.myretroe.2019.01.016.
- Petrol. Geol. 102, 704–724. https://doi.org/10.1016/j.marpetgeo.2019.01.016.
 Zhang, Q.P., Liu, Y.C., Wang, B.T., et al., 2022a. Effects of pore-throat structures on the fluid mobility in chang 7 tight sandstone reservoirs of Longdong area, Ordos Basin. Mar. Petrol. Geol. 135, 105407. https://doi.org/10.1016/j.marpetgeo.2021.105407.
- Zhang, Q.T., Liu, W.C., Taleghani, A.D., 2022b. Numerical study on non-Newtonian Bingham fluid flow in development of heavy oil reservoirs using radio-frequency heating method. Energy 239, 122385. https://doi.org/10.1016/j.energy.2021.122385.
- Zhao, W.Z., Hu, S.Y., Hou, L.H., et al., 2020. Types and resource potential of continental shale oil in China and its boundary with tight oil. Petrol. Explor. Dev. 47 (1), 1–11. https://doi.org/10.1016/S1876-3804(20)60001-5.
- Zhao, W.Z., Zhu, R.K., Liu, W., et al., 2023. Lacustrine medium-high maturity shale oil in onshore China: enrichment conditions and occurrence features. Earth Sci. Front. 30 (1), 116–127. https://doi.org/10.13745/j.esf.sf.2022.8.31 (in Chinese).
- Zhu, W.Y., Liu, Y.W., Shi, Y.Q., et al., 2022. Effect of dynamic threshold pressure gradient on production performance in water-bearing tight gas reservoir. Adv. Geo-Energy Res. 6 (4), 286–295. https://doi.org/10.46690/ager.2022.04.03.
- Zou, C.N., Yang, Z., Sun, S.S., et al., 2020a. "Exploring petroleum inside source kitchen": Shale oil and gas in Sichuan Basin. Sci. China Earth Sci. 63 (7), 934–953. https://doi.org/10.1007/s11430-019-9591-5 (in Chinese).
- Zou, C.N., Pan, S.Q., Jing, Z.H., et al., 2020b. Shale oil and gas revolution and its impact. Acta Petrol. Sin. 41 (1), 1–12. https://doi.org/10.7623/syxb2020010 (in Chinese).